Investigation of Mercury Green and Yellow Lines, and White Light Fringes with the Michelson Interferometer

Brian Lim and D. L. Hartill

Cornell University, Ithaca, New York 14853, USA

(Received 3 October 2005)

The Michelson interferometer was calibrated using the mercury green line and the lever calibration factor was found to be $K = 0.207 \pm 0.003$. Knowing this, interference fadeouts due to the mercury yellow doublet was measured with respect to mirror displacement to determine the wavelength difference between the yellow lines. The wavelength difference is reported as $\Delta\lambda_y = 2.10 \pm 0.04\,\text{nm}$. Finally, zero path difference was achieved and white light fringes observed at screw gauge reading $g = 16.600 \pm 0.005\,\text{mm}$.

1. Introduction

Invented around the 1880s , the Michelson interferometer has been an indispensable tool in many areas of Physics, including interferometry, spectroscopy and special relativity. For example, it was used in the Michelson-Morley experiment and failed to demonstrate the presence of an ether for light to travel in, paving the way for the theory of special relativity. More importantly, though, is the application of the Michelson interferometer in interferometry. Prior to its existence, scientists used slits, lenses and mirrors to investigate interference, such as the Young's double slit, Fresnel's biprism and Lloyd's mirror. An important requirement for interference that these tools satisfy is that the interference beams originate from the same source, so they are coherent. If not, random fluctuations in phase shifts would cause the light rays to be out of phase in an inconsistent manner. However, the light paths for the aforementioned equipment are not parallel when they interfere at the detector, so the maximum path difference between them is limited.

The Michelson interferometer satisfies the requirement for a single light source, by taking a beam and splitting it with a beamsplitter and ultimately recombining them, with the use of mirrors, at the detector. This allows the beams to be parallel so that path differences can be longer (~0.5m). It relies on moving one of two mirrors to adjust the path difference between the two light beams.

However, given the very small scale of optical wavelengths (~100nm) compared to what we can move with our fingers (~5mm), the movement of this mirror is scaled via a micrometer screw gauge and a lever. There is a conversion factor of about 0.2 for modern interferometers as shown in Figure 2.2.

An important application of observing the interference is the study of atomic spectra. When ionized at high temperatures, atomic gases would emit radiation, due to excited electrons returning to lower energy levels and releasing photons. Since the energy levels are quantized and discrete, the radiation emitted (which falls within the optical range) consists of distinct bands of color. By studying the interference pattern formed from such radiation, it is possible to infer the wavelengths of the spectra and thus the energy levels of various atoms. Thus the Michelson interferometer can reveal the constituents of each atomic spectra.

More generally, interferometry can also be used to investigate the constituents of any source. For example, it can reveal the spectrum of white light, showing the colors that make it up.

2. Description of Apparatus

The interferometer employed was manufactured by Earling (SN G-035), owned by Cornell University Physics Department. As described by Andrews and Luther[1], and illustrated in the schematic in Figure 2.1 and the picture in Figure 2.2, the generic Michelson interferometer is made up of the following:

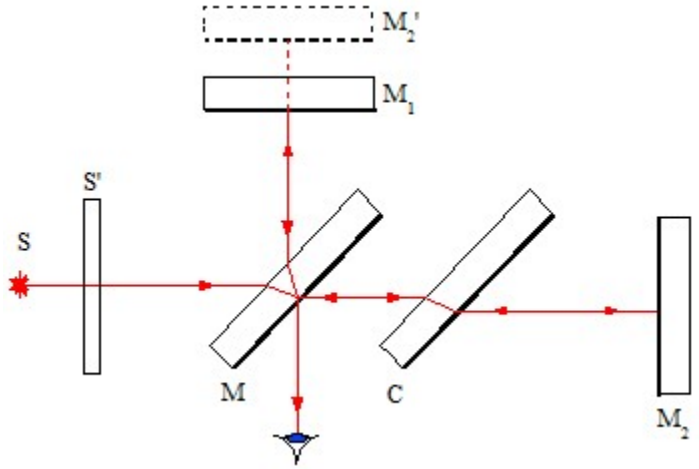

Figure 2.1: Michelson interferometer schematic

- ***S***, light source

  This provides the single coherent source, a mercury lamp or a white light bulb for this lab.

- ***S'***, ground-glass screen to provide an extended plane source

  Since pin sources would not form observable interference patterns, an extended light source is needed. This glass screen disperses the light to simulate an extended source. Filters to reduce the spectral range of the source can be placed after this screen, before *M*.

- ***M***, beamsplitter

  Half-silvered with an aluminum coat on one face, this splits the source beam into two parts, one reflecting off at 90° from its original direction towards M_1, and the other transmitting through towards *C* and M_2.

- ***C***, compensating glass

  This is cut from the same glass as *M*, to ensure the same thickness, so that both split beams travel through the same distances in glass, i.e. goes through glass three times.

- $\boldsymbol{M_1}$, movable mirror

  Moving this mirror would change the path distance of the beam traveling along the path going up, causing the interference fringes to move too.

- $\boldsymbol{M_2}$, the other mirror which can be tilted vertically and horizontally

  This mirror is not able to move laterally, but can be tilted horizontally and vertically using the 2 knobs which can be seen in Figure 2.2. This allows for localized fringes (fringes that appear almost vertical, since they are arcs of circular fringes with very large radii) to be viewed, such that straight (vertically, horizontally, or a combination of both) fringes, rather than circular, can also be observed.

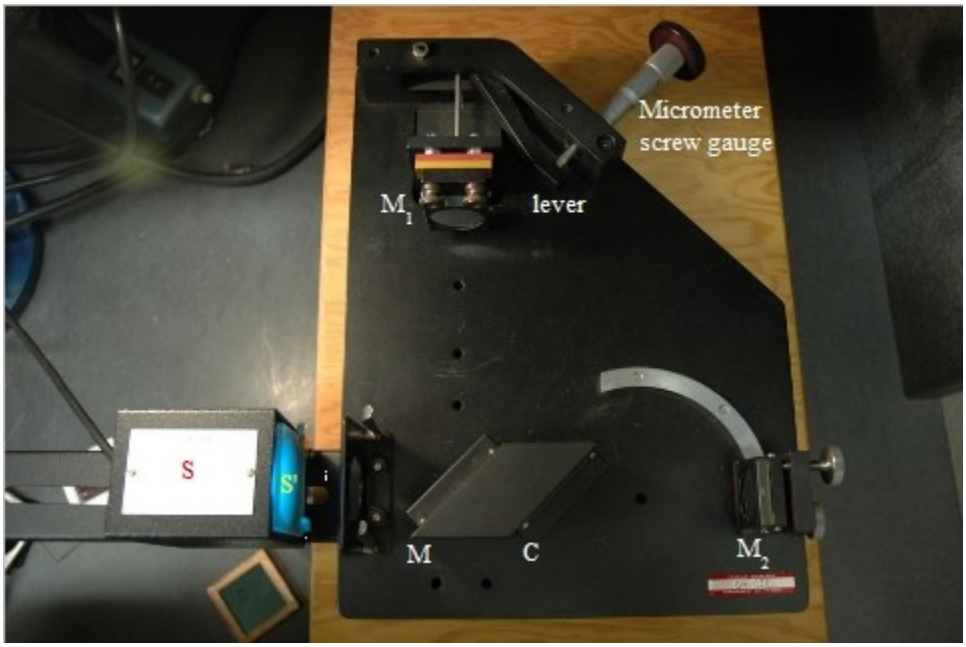

Figure 2.2: Michelson interferometer apparatus

There are various ways to move mirror M_1, and they generally involve turning a micrometer screw gauge so that finer movement of the mirror can be achieved. However, care should be taken to turn the screw in the same direction while taking readings, as hysteresis effects can lead to systematic errors. To improve the precision of moving M_1, newer interferometers, such as the one we used, employs a lever that further reduces the mirror movement by a lever calibration factor, K (~0.2).

3. Theory

For a coherent light source, interference fringes form because of the path difference, l,

between the light beams arriving at each point on the detector. Light arriving at each point would be at different phases and interfere differently. In particular, when the path difference, l, is a multiple of the wavelength, i.e.

$$l = n\lambda, \quad n \in \mathbb{Z} \tag{3.1}$$

constructive interference occurs, giving a bright fringe, and when

$$l = \frac{2n+1}{2}\lambda, \quad n \in \mathbb{Z} \tag{3.2}$$

there is destructive interference, giving a dark fringe. However, the path difference between fringes are the same for bright and dark

$$\Delta l = \Delta n \lambda, \quad n \in \mathbb{Z} \tag{3.3}$$

The following derives the theoretical workings of the interferometer[1,2]. The paths the split beams of the Michelson interferometer can be though of as if aligned along the same axis as shown in Figure 3.1. S_1 is the image of the source, S', that can be seen due to M_1, while S_2 is the image of S' reflected in M_2. The difference in distance of both mirrors, M_1 and M_2, from the source S' is d.

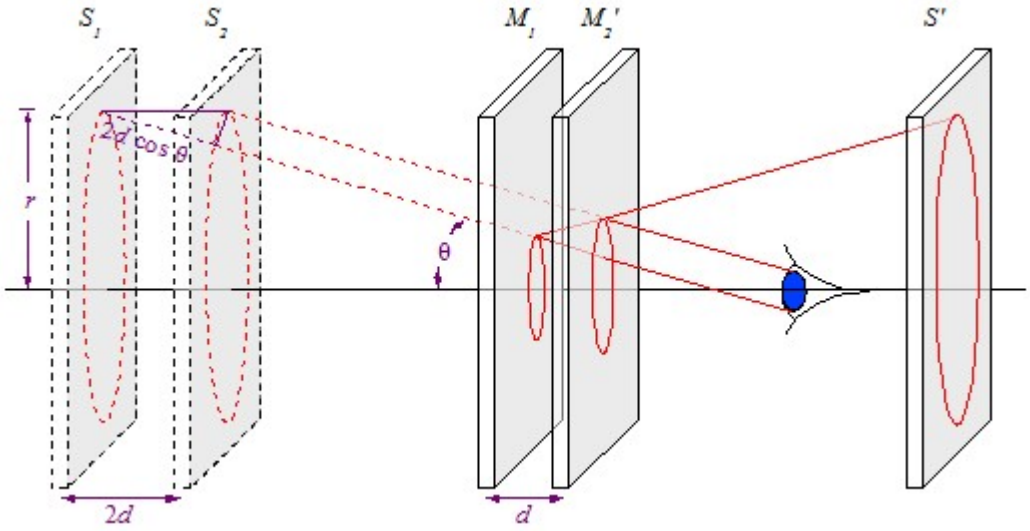

Figure 3.1: Diagram of optical paths with virtual images

As can be seen from Figure 3.1, the path difference is

$$l = 2d\cos\theta \tag{3.4}$$

Combining this with Equation 3.1 and 3.3 gives the useful equation

$$2D\cos\theta = N\lambda\,, \quad D = \Delta d\,, N = \Delta n \tag{3.5}$$

When small circular fringes are observed near the center of the image (i.e. negligible radius r), $\theta \approx 0$, so $\cos\ \theta \approx 1$ and Equation 3.5 reduces to

$$\lambda = \frac{2D}{N} \tag{3.6}$$

Thus the wavelength of a coherent light source can be determined from observing N fringes move by and measuring the distance mirror M_1 moved.

3.2. Measurement of Wavelength Difference

Figure 3.2 illustrates that two very close wavelengths would interfere to form beats. In optical interference, these beats can be observed by seeing fadeouts where the fringing is least distinct.

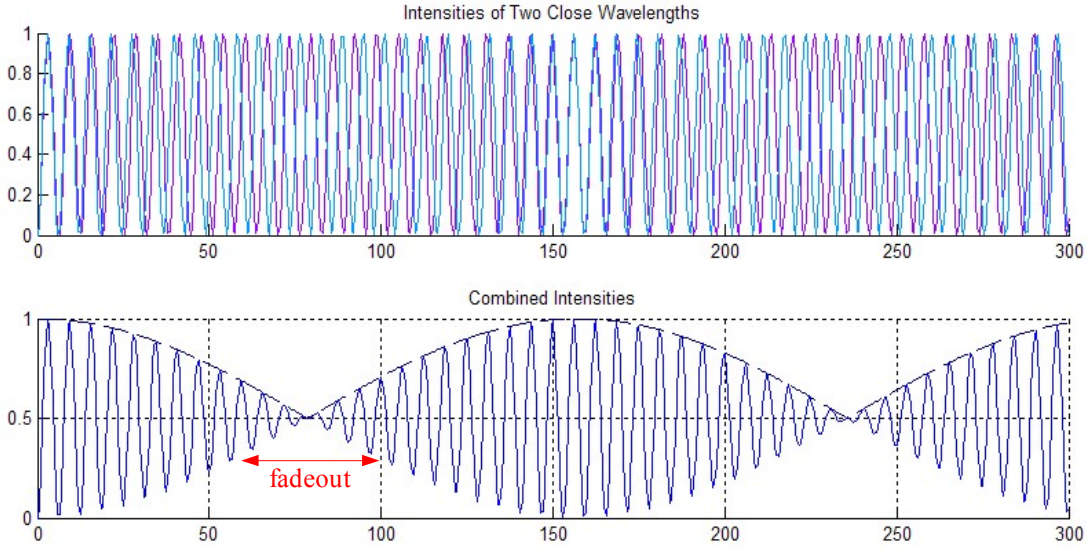

Figure 3.2: Graphs of interference to form fadeouts

[1]The middle of each fadeout occurs when both waves are anti-phase, so from Equations 3.1 and 3.4,

$$2d_n = m_n\lambda = (m_n - \frac{2n-1}{2})\lambda' \quad (3.7)$$

where λ is shorter than λ' by Δλ and m_n is the number of fringes up to the middle of the n^{th} fadeout and d_n is the distance to that point. In particular, for $n = 1$:

$$2d_1 = m_1\lambda = (m_1 - \frac{1}{2})\lambda' \quad (3.8)$$

such that $\Delta\lambda = \lambda\lambda'/4d_1$. and with $\lambda \approx \lambda'$, $\Delta\lambda \approx \lambda^2/4d_1$.

Subtracting λ from λ' gives, and after some work,

$$\Delta\lambda = \frac{\lambda\lambda'(2n-1)}{4d_n} \quad (3.9)$$

At the k^{th} fadeout,

$$\Delta\lambda = \frac{\lambda\lambda'(2k-1)}{4d_k} \quad (3.10)$$

Taking the differences $N = n - k$ and $D = d_n - d_k$, and substituting λ and λ' for $\overline{\lambda}$,

$$\Delta\lambda = \frac{\overline{\lambda}^2 N}{2D} \quad (3.11)$$

This equation can give the wavelength difference between doublets in an interference spectrum.

3.3. White Light Fringes

An important task that the Michelson interferometer can accomplish is to reveal the spectrum of light. At zero path difference, white light would split up visibly into its constituent colors, as shown in Figure 3.3, constructed using wavelength values of various colors[3] and the equation $c = \nu\lambda$, relating the speed, frequency and wavelength of a wave. This diagram shows white light fringes with a central black fringe due to the phase change, of 180°, of one of the light beams (as described in Section 2). As described by Jenkins and White[4], after about 9 fringes, so many colors are present at every point that it appears a low contrast white. Therefore, it becomes practically impossible to view

the white light fringes beyond that, and thus it is also a relatively non-trivial task to locate the zero path difference. However, once determined, the zero path difference is the best position to conduct measurements at.

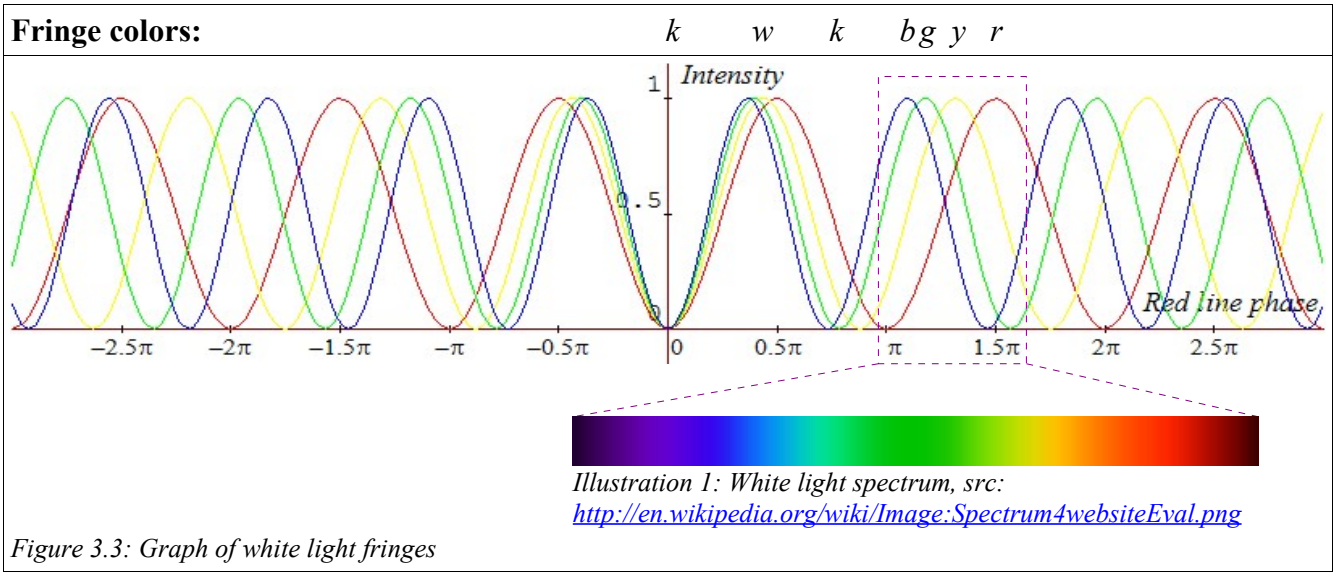

Illustration 1: White light spectrum, src: *http://en.wikipedia.org/wiki/Image:Spectrum4websiteEval.png*

Figure 3.3: Graph of white light fringes

4. Procedure

As there are three objectives for this lab, it is subdivided into three experiments: 1a, 1b, and 1c. Experiment 1a involves the calibration of the Michelson interferometer using the mercury green line, Experiment 1b involves the determination of the wavelength difference between the two mercury yellow lines of average wavelength[5] 578.012nm, and experiment 1c involves observing white light fringes, which can only be seen very near to zero path difference.

4.1. Experiment 1a: Calibration of lever to find *K*

Placing a green filter in front of a mercury source allows the fringes of the 546.074nm green wavelength[5] . It is best to adjust the tilt of mirror M_2 such that small circular fringes are observed, so that mathematical approximations in the theory are valid. Moving M_1 to adjust the path difference by turning the micrometer screw gauge, would make the fringes appear to move. Counting the fringes that moves pass a certain point in the image, or collapse to/expand from a point, and noting the change in

screw gauge reading would allow one to correspond fringe count to screw gauge movement. Knowing the wavelength of the source and this correlation, one can calculate the calibration factor, K, of the lever that scales the gauge screw movement to mirror movement.

4.2. Experiment 1b: Determination of $\Delta\lambda$

To view the fadeouts in the fringes due to a pair of doublet wavelengths, it is easier to use of localized fringes (straight lines) than circular ones. This can be seen by tilting mirror M_2. Since many fringes pass between each fadeout, it is possible to move the screw gauge at a faster rate than in Experiment 1a. By measuring the gauge reading difference at each fadeout, the relation between fadeout count and gauge reading can be ascertained. Using K found from experiment 1a, the difference between the mercury yellow doublet lines, $\Delta\lambda$, can be calculated.

4.3. Experiment 1c: Observation of white light fringes

White light fringes can only be observed for up to about 9 fringes away from zero path difference making finding them relatively difficult to view. To begin, the path difference can be made roughly close to zero by using a ruler and moving M_1 such that the paths are about the same length. Then, using another light source, the zero path difference can be more accurately obtained. Once again, localized fringes would be more useful than circular ones. There are two techniques to help find zero path difference. The first notes that localized fringes are actually arc-like but get straighter as the path difference goes to zero, and curve more in the other direction as the path difference passes it. Secondly, if a multicolored source is used, the colored fringes would also change order on the opposite side of zero path difference. Thus a mercury source without filter would be suitable. When the path difference

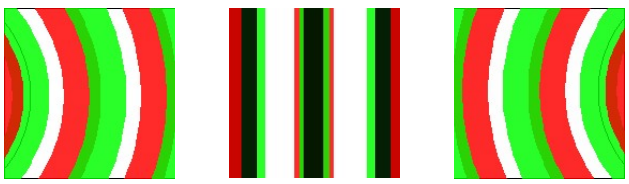

Figure 4.3.1: Fringes become straighter towards zero path difference and fringe sequences are reversed on opposite sides of it

is close to zero, then the source can be switched to the white light, and slowly moving M_1 should help one arrive to find the white light fringes eventually.

5. Data

For Experiment 1a, the micrometer gauge reading is recorded after every 50 fringes are counted, for up to 1200 fringes each run. This is presented in the table in Appendix A, page I. The first few runs were conducted at random mirror positions, the next few near zero path difference, and the last 5 about zero path difference. The dates on which the runs were conducted are recorded at the bottom of each table. Table 5.1 shows raw and preprocessed data for runs 8 to 11.

Fringes, *i* (exact)	Gauge Reading, g (mm) (all ± 0.005 mm)					Difference, $\Delta g = g_i - g_{i-1}$ (mm) (all ± 0.010 mm)			
	8	9	10	11		8	9	10	11
0	17.400	17.400	17.400	17.400					
50	17.335	17.335	17.335	17.335		0.065	0.065	0.065	0.065
100	17.270	17.270	17.270	17.265		0.065	0.065	0.065	0.070
150	17.205	17.205	17.205	17.200		0.065	0.065	0.065	0.065
200	17.140	17.135	17.140	17.135		0.065	0.070	0.065	0.065
250	17.070	17.070	17.070	17.070		0.070	0.065	0.070	0.065
300	17.005	17.005	17.005	17.005		0.065	0.065	0.065	0.065
350	16.940	16.940	16.940	16.940		0.065	0.065	0.065	0.065
400	16.875	16.870	16.875	16.870		0.065	0.070	0.065	0.070
450	16.810	16.805	16.810	16.805		0.065	0.065	0.065	0.065
500	16.745	16.740	16.740	16.740		0.065	0.065	0.070	0.065
550	16.675	16.670	16.675	16.670		0.070	0.070	0.065	0.070
600	16.610	16.605	16.610	16.605		0.065	0.065	0.065	0.065
650	16.545	16.540	16.545	16.540		0.065	0.065	0.065	0.065
700	16.480	16.475	16.480	16.475		0.065	0.065	0.065	0.065
750	16.410	16.410	16.415	16.410		0.070	0.065	0.065	0.065
800	16.345	16.340	16.350	16.340		0.065	0.070	0.065	0.070
850	16.280	16.275	16.280	16.275		0.065	0.065	0.070	0.065
900	16.210	16.205	16.215	16.210		0.070	0.070	0.065	0.065
950	16.145	16.140	16.150	16.140		0.065	0.065	0.065	0.070
1000	16.075	16.070	16.080	16.075		0.070	0.070	0.070	0.065
1050	16.010	16.005	16.020	16.010		0.065	0.065	0.060	0.065
1100	15.945	15.940	15.950	15.945		0.065	0.065	0.070	0.065
1150	15.880	15.875	15.885	15.880		0.065	0.065	0.065	0.065
1200	15.815	15.810	15.820	15.810		0.065	0.065	0.065	0.070

Table 5.1: Experiment 1a; raw and preprocessed data

For Experiment 1b, gauge readings are recorded and presented in Appendix A, page III.

The first run involves measuring at every 5 fadeouts throughout the whole range of the screw gauge (0.00mm to 25.00mm). Runs 2 and 3 measure readings at every fadeout over shorter random ranges of mirror movements. Runs 4 to 8 measure readings at every fadeout for even shorter ranges near zero path difference. Runs 9 to 16 measure readings at every fadeout for the gauge reading range ~15.65mm to ~17.55mm, which is about zero path difference.

Fadeouts, i (exact)	Gauge Reading, g (mm) $(\text{all} \pm 0.01\,\text{mm})$								Difference, $\Delta g = g_i - g_{i-1}$ (mm) $(\text{all} \pm 0.02\,\text{mm})$							
	9	10	11	12	13	14	15	16	9	10	11	12	13	14	15	16
0	17.58	17.58	17.56	17.54	17.55	17.54	17.54	17.54								
1	17.19	17.20	17.19	17.16	17.16	17.17	17.16	17.16	0.39	0.38	0.37	0.38	0.39	0.37	0.38	0.38
2	16.81	16.80	16.81	16.77	16.77	16.78	16.77	16.77	0.38	0.40	0.38	0.39	0.39	0.39	0.39	0.39
3	16.43	16.43	16.43	16.38	16.38	16.39	16.38	16.38	0.38	0.37	0.38	0.39	0.39	0.39	0.39	0.39
4	16.04	16.04	16.03	16.00	16.00	16.00	16.00	16.00	0.39	0.39	0.40	0.38	0.38	0.39	0.38	0.38
5	15.66	15.66	15.65	15.61	15.61	15.61	15.62	15.61	0.38	0.38	0.38	0.39	0.39	0.39	0.38	0.39

Table 5.2: Experiment 1b; raw and preprocessed data

For Experiment 1c, zero path difference was found at gauge reading, 16.600 ± 0.005 mm, and white light fringes were observed around that. The center fringe was black, flanked by two white fringes, followed by black again. Multicolored fringes (order: yellow, red, blue, green) were observed alternating with white for about 4 fringes from the central fringe. Subsequently, only red fringes alternating with green fringes were visible for up to 6 more fringes. In total, 10 red fringes in from gauge reading 16.590 ± 0.005 to zero path difference and 9 from there to 16.610 ± 0.005 were visible before they become indistinguishable from a uniform white.

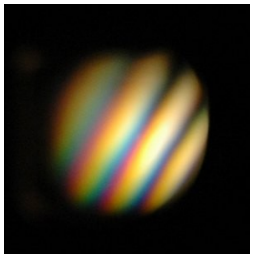

Figure 5.1: Multicolored fringes at zero path difference

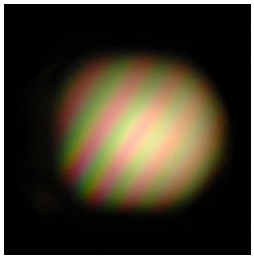

Figure 5.2: Red and green fringes near zero path difference

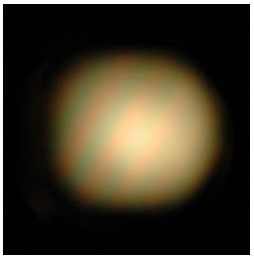

Figure 5.3: Faint red and green fringes farther from zero path difference

Images of such white light fringes and the full mercury spectrum were captured on digital

cameras. The fringe images appear noticeably different when captured on the different cameras. Images taken with the Fuji Finepix S602 are in Appendix B, and images taken with the Nikon D70 are in Appendix C.

6. Data Analysis & Discussion

Appendix A has two tables, on pages II and IV, listing the difference between consecutive gauge readings. Appendices D-F provide graphical and statistical analyses of all the runs, studied individually or in groups, of Experiments 1a and 1b. Runs 8-11 of Experiment 1a are most appropriate since they are closest to zero path difference and do not exhibit hysteresis. As a result, only runs 2, 9, and 9-11 of Experiment 1b are valid, since only they fall in the calibration range of Experiment 1a. Also note that since the errors in the gauge readings are Gaussian distributed, all derived parameters are also Gaussian distributed.

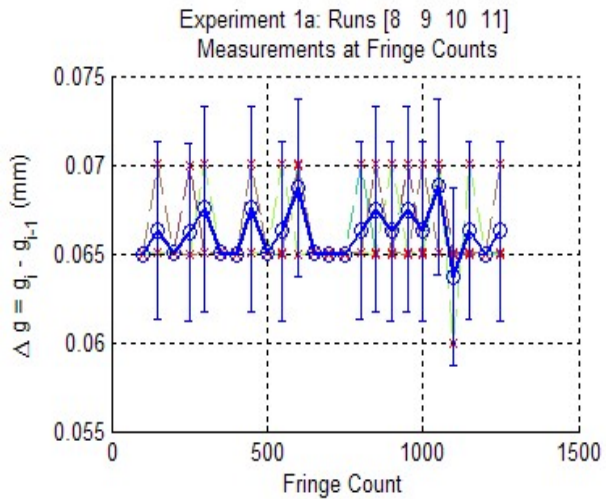

Figure 6.1.1: Fluctuations of gauge reading difference for Experiment 1a

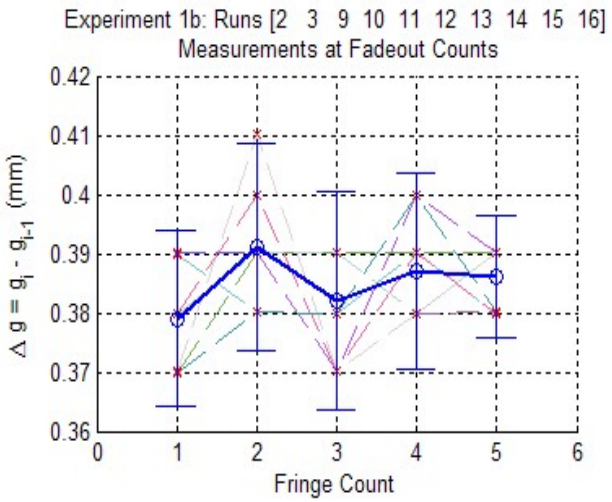

Figure 6.1.2: Fluctuations of gauge reading difference for Experiment 1b

6.1.1. Comment on Hysteresis

In Experiment 1a, runs 5-7 had unstable fluctuations for the first few points because of

hysteresis. This was due to having turned the screw gauge knob one direction while setting mirror M_1, and then turning in the opposite direction to start take readings. This lead to hysteresis in the screw and lever that are manifested by the initially high values of Δg followed by particularly low readings. However, the effect diminished after about 6 readings. By ensuring to start the screw gauge turning in one direction before taking readings, these effects of hysteresis were eliminated for future runs.

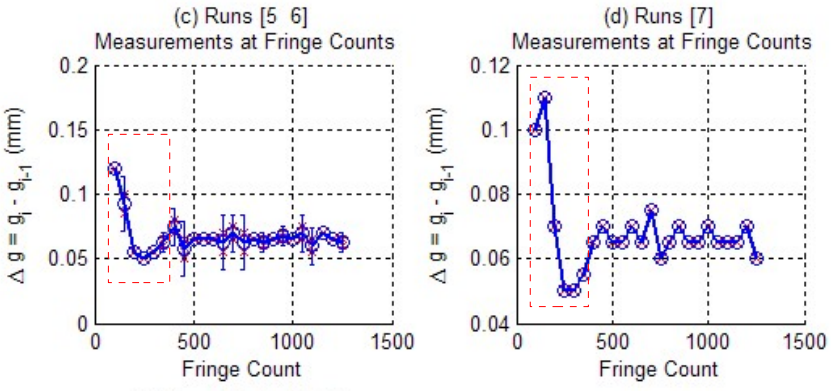

Figure 6.1.3: Effects of hysteresis

6.1.2. Determination of *K*, the lever conversion factor

Using just runs 8-11 conducted around zero path difference, the value of K is determined from 4 runs with 96 data points in all. The lever relates screw gauge movement to mirror displacement by $d = Kg$. Substituting this into equation 3.6 and rearranging would produce

$$K = \frac{\lambda_g N}{2\Delta g} \qquad (6.1.1)$$

$N = 50$, since 50 fringes were counted between each measurement, and $\lambda_g = 546.074$nm, the accepted wavelength of the mercury green line[5].

Calculating via quadrature from Table 5.1, the uncertainty in $\overline{\Delta g}$ is

$$\delta(\overline{\Delta g})_{table} = \frac{1}{N}\sqrt{\sum_1^N \delta(\Delta g)_i^2} = \frac{1}{96}\sqrt{96 * 0.01^2} = 0.0010\,\text{mm}$$

However, statistically, the standard deviation of the weighted mean of Δg is 0.0011mm, which is

larger than, but close to, $\delta\overline{(\Delta g)}^{(a)}_{table}$. So take the standard deviation as the proper error. Therefore, the weighted mean is $\overline{(\Delta g)}^{(a)}_{weighted} = 0.0661 \pm 0.0011$ mm. The uncertainty in K is calculated to be

$$\delta K = \sqrt{\left(\frac{\partial K}{\partial \lambda_g}\right)^2 (\delta \lambda_g)^2 + \left(\frac{\partial K}{\partial (\Delta g)}\right)^2 (\delta(\Delta g))^2} = \sqrt{\left(\frac{N}{2\Delta g}\right)^2 (\delta \lambda_g)^2 + \left(-\frac{\lambda N}{2(\Delta g)^2}\right)^2 (\delta(\Delta g))^2}$$
$$= 0.0034$$

So, the interferometer is calibrated with $K = 0.207 \pm 0.003$.

6.2.1. Determination of $\Delta\lambda_y$, difference in wavelength of the mercury yellow doublet

Applying similar analysis to data from Experiment 1b, the weighted mean of gauge reading differences is $\overline{(\Delta g)}^{(b)}_{weighted} = 0.386 \pm 0.002$ mm. Since the accepted mercury yellow lines[5] have wavelengths 576.959nm and 579.065nm, their average is $\overline{\lambda_y} = 578.012$ nm. From Equation 3.6, with $D = K\overline{(\Delta g)}^{(b)}_{weighted}$, $N = 1$ and $\lambda = \overline{\lambda_y}$, the uncertainty in $\Delta\lambda_y$ is

$$\delta(\Delta\lambda_y) = \sqrt{\left(\frac{\partial(\Delta\lambda_y)}{\partial \overline{\lambda_y}}\right)^2 (\delta \overline{\lambda_y})^2 + \left(\frac{\partial(\Delta\lambda_y)}{\partial K}\right)^2 (\delta K)^2 + \left(\frac{\partial(\Delta\lambda_y)}{\partial g}\right)^2 (\delta(\Delta g))^2}$$
$$= \sqrt{\left(\frac{\overline{\lambda_y} N}{K\Delta g}\right)^2 (\delta \overline{\lambda_y})^2 + \left(-\frac{\overline{\lambda_y}^2 N}{2K^2 \Delta g}\right)^2 (\delta K)^2 + \left(-\frac{\overline{\lambda_y}^2 N}{2K(\Delta g)^2}\right)^2 (\delta(\Delta g))^2}$$
$$= 0.036 \text{ nm}$$

Finally, using equation 3.6 gives $\Delta\lambda_y = 2.096 \pm 0.036 \approx 2.10 \pm 0.04$ nm.

6.2.2. Hypothesis testing of $\Delta\lambda_y = 2.106$ nm at 10% level of significance

Using the accepted values of mercury yellow lines[5] would give $\Delta\lambda_y = 2.106$ nm. The following proceeds to check if Experiment 1b achieved this result within a 10% level of significance.

$$H_0 : \Delta\lambda_y = 2.106 \text{ nm}$$
$$H_1 : \Delta\lambda_y < 2.106 \text{ nm}$$
$$Z = \frac{\Delta\lambda_y - 2.106}{0.036} \sim N(0,1)$$
$$< -Z_{1-\alpha} = -1.282, \quad \alpha = 10\%$$
$$\Delta\lambda_y < -0.036 * Z_{1-\alpha} + 2.106 = 2.060 \text{ nm}$$

=> at 10% level of significance, $\Delta\lambda_y = 2.10 \pm 0.04$ nm is still acceptable, off from the accepted value by 0.475%.

6.3.1. Explanation for central black fringe of white light fringes

For this interferometer, *M* is half-silvered with an aluminum coat, with refractive indices[6] $n_{Al} \approx 1.39$, $n_{Al_2O_3} \approx 1.79$, and $n_{glass} \approx 1.5$, and $n_{air} = 1.00029$. Even though the outer layer of the aluminum coat is oxidized, the surface in contact with the glass is preserved. As described by Griffith[7], the reflected amplitude to the incident amplitude by

$$\tilde{E}_{0_R} = \left(\frac{n_1 - n_2}{n_1 + n_2} \right) \tilde{E}_{0_I}$$

So for light reflecting from air onto the silvered surface, $n_1 = n_{air}$ and $n_2 = n_{Al_2O_3}$, causing the reflected wave to be phase shifted by 180°; for reflection within the glass, $n_1 = n_{glass}$ and $n_2 = n_{Al}$, giving rise to no phase change. Thus one path is phase changed relative to the other and at zero path difference, the light beams would interfere destructively, producing a central black fringe.

6.3.2. Verification of measurements in observing white light fringes

Since the screw gauge range 16.590 ± 0.005 mm to 16.610 ± 0.005 mm marks the region of visible white fringes, the gauge reading varies by $\pm(0.010 \pm 0.010)$ mm from the gauge reading at zero path difference, 16.600 ± 0.005 mm . The relation $D = K \Delta g$ gives

$$\delta D = \sqrt{\left(\frac{\partial D}{\partial K} \right)^2 (\delta K)^2 + \left(\frac{\partial D}{\partial g} \right)^2 (\delta(\Delta(\Delta g)))^2} = \sqrt{(\Delta g)^2 (\delta K)^2 + (K)^2 (\delta(\Delta g))^2}$$
$$= 2.07 \mu\text{m}.$$

With the value of K determined in 6.1.2, it is calculated that white fringes were visible with path differences within the range $\pm(2.1 \pm 2.1)\mu$m . Assuming the wavelength of the red fringe is 650nm[3], Equation 3.6 would suggest a fringe count of 6.5 ± 6.5 (i.e. between 0 to 13) either way from zero path difference. Therefore, the actual fringe count of 9 and 10 from zero path difference is acceptable, given

the limited accuracy.

6.3.3. Mapping of photographs white light fringes to graphical model

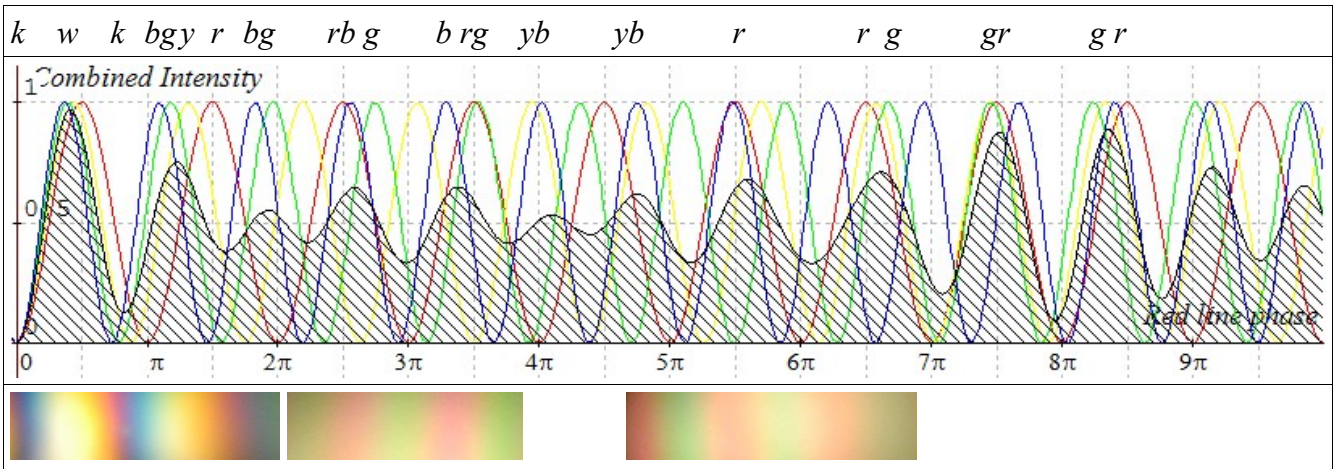

Figure 6.3.1: Mapping observed fringes to graphical model

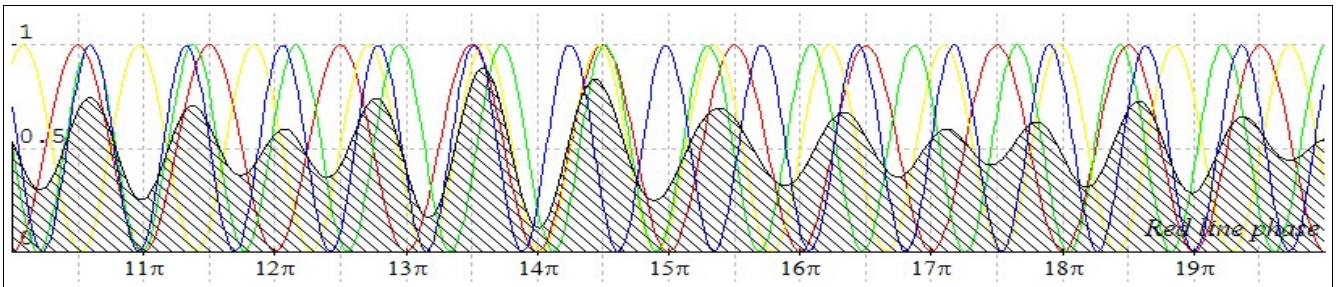

Generally low contrast white from this far onwards →
Figure 6.3.2

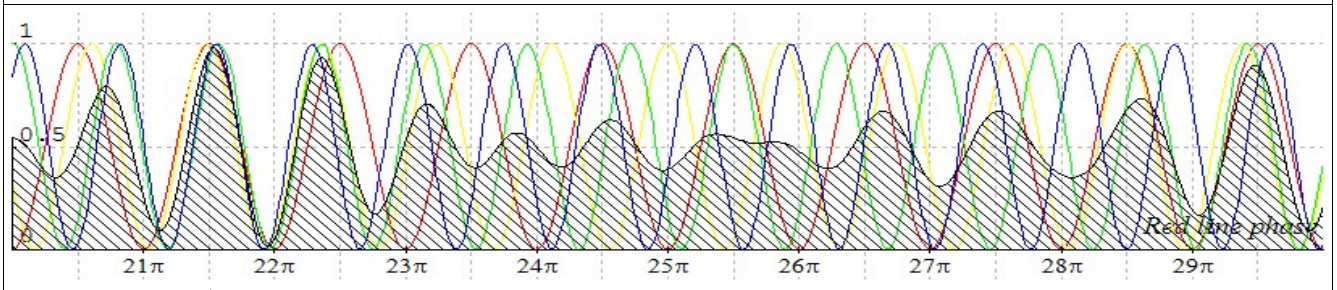

↑ bright fringe here only visible if mirrors are perfect
Figure 6.3.3

The captured images of white light fringes are compared against theoretical graphs as in Figures 6.3.1-6.3.3, extensions of Figure 3.3. By mapping some clippings of pictures of the fringes to the graphs for the first 8 fringes, there appears to be reasonable agreement. Bright fringes would correspond to the maxima of the the combined intensity (shaded black curve); dark fringes would

correspond to the minima. Note, though, of the chromatic aberration (darkening) at the edges of the photographs and white lens glares at the middle. To the right of the images would be the yellowish low contrast white light where too many colors wash out one another to become indistinguishable.

According to the theoretical graph of Figure 6.3.3, at 21.5π, there should be a bright fringe surrounded by two dark fringes. However, this was not found experimentally, since the imperfections in the mirrors create uncertainties to diminish the effects of this interference.

As expected according to what was described in 6.3.1, the central fringe is dark because of the aluminum oxide coating on one side of the beamsplitter.

7. Conclusion

The experiments conducted in this lab successfully calibrated the Michelson interferometer with the mercury green line, and used it to determine the difference in the wavelengths of the mercury yellow doublet. Zero path difference was obtained and white light fringes observed to fit well with the theoretical model. The lever calibration factor was found to be $K = 0.207 \pm 0.003$, the mercury yellow doublet wavelength difference measured to be $\Delta \lambda_y = 2.10 \pm 0.04 \text{ nm}$, and zero path difference determined at gauge reading $16.600 \pm 0.005 \text{ mm}$, with up to 10 visible white fringes around it.

Still, some issues were brought up that could require further investigation. The effects of hysteresis can be more thoroughly studied to find out the extent to which it affects the readings. Also, as elaborated in Appendix H, *K* was found to vary with gauge screw position, but this could be more properly investigated. Finally, the calibration could be further verified by using a coherent source, such as a laser, or another frequency of light.

Acknowledgements

Special thanks goes out to Prof Hartill for his guidance, Prof Hand for his help on how to analyze the data and his imparting of the experimentalist ideal of not assuming properties in the apparatus and on preserving the integrity of all data collected, and Ava Wan for helping to clarify what to do for the first part of this lab, i.e. to calibrate the interferometer.

---

[1]Andrews, C. Luther, Optics of the electromagnetic spectrum, Chap. 7, Prentice-Hall, 1960.

[2]Wood, Physical Optics, pp. 292-305, (3rd Edition).

[3]Barkstrom, What Wavelength Goes With a Color? Atmospheric Sciences Data Center, Nasa, retrieved from http://eosweb.larc.nasa.gov/EDDOCS/Wavelengths_for_Colors.html, on Oct 01, 2005.

[4]Jenkins and White, Fundamentals of Optics, Chap. 13.

[5]Jenkins and White, Fundamentals of Optics, Chap. 21, (4th Edition), McGraw-Hill, 1976.

[6]B. V. Zeghbroeck, Principles of Semiconductor Devices, 1997, retrieved from http://ece- www.colorado.edu/~bart/book/ellipstb.htm, on Oct 01, 2005.

[7]Weisstein, Index of Refraction, retreived from http://scienceworld.wolfram.com/physics/IndexofRefraction.htm, on Oct 01, 2005.

[8]D. J. Griffiths, Introduction to Electrodynamics, pp. 386-392, (3rd Edition).